ELSEVIER

Thermochimica Acta 387 (2002) 109–114

thermochimica acta

www.elsevier.com/locate/tca

Short communication

Non-isothermal studies of the decomposition course of lanthanum oxalate decahydrate

Basma A.A. Balboul[a,*], A.M. El-Roudi[a], Ebthal Samir[a], A.G. Othman[b]

[a]*Chemistry Department, Faculty of Science, Minia University, El-Minia 61519, Egypt*
[b]*Ceramic Department, Natural Research Center, Dokki, Cairo, Egypt*

Received 28 June 2001; received in revised form 23 October 2001; accepted 25 October 2001

Abstract

The thermal decomposition of lanthanum oxalate hydrate $La_2(C_2O_4)_3{\cdot}10H_2O$ till 900 °C, in air, is investigated by non-isothermal gravimetry and differential thermal analyses. Intermediates and final solid products were characterized by X-ray diffraction (XRD) and IR-spectroscopy, the results show that $La_2(C_2O_4)_3{\cdot}10H_2O$ dehydrates in stepwise at 86–360 °C and decomposes to La_2O_3 at 710 °C through different intermediates, $La_2(C_2O_4)_3$, $La_2O(CO_3)_2$ and $La_2O_2CO_3$, that form at 400, 425 and 470 °C, respectively. The final product La_2O_3 obtained at 800 °C has a surface area of 13.4 m^2/g. The activation energy, ΔE of the observed thermal processes is obtained by the non-isothermal method.

Keywords: La-oxalate; La-oxide; Decomposition; DTA; TG; IR; XRD; S_{BET}

1. Introduction

The hexagonal [1] structure, lanthanum sesquioxide, La_2O_3, the final decomposition course studied in the present investigation, is the only stable oxide of lanthanum up to 2050 °C. La_2O_3 has numerous applications in various industrial and the technological fields. It is an important component of automobile exhaust—gas conversion [2], as a catalyst support in the formation of gas conversion catalyst [3,4], and as a catalyst of oxidative coupling of methane [5–7]. It is also used as a refractory oxide for calcium lights, optical glass [8], and in the formation of ceramics as a core for carbon arc electrodes [8].

The aim of the present study is to characterize the thermal decomposition of $La_2(C_2O_4)_3{\cdot}10H_2O$ to the onset of La_2O_3 by means of thermogravimetry (TG) and differential thermal analysis (DTA). The solid products of the reaction were analyzed by IR-spectroscopy and X-ray diffractometry. The surface area (S_{BET}) was measured by N_2-adsorption isotherm. The activation energy, ΔE of the observed thermal processes is obtained by the non-isothermal method of thermoanalytical data analysis.

2. Experimental

2.1. Materials

Lanthanum acetate tetrahydrate (LaAc, $La(CH_3COO)_3{\cdot}4H_2O$) (99.9% pure from Aldrich, USA),

* Corresponding author. Tel.: +20-86-34-52-31; fax: +20-86-34-26-01.
E-mail address: bsman64@yahoo.com (B.A.A. Balboul).

0040-6031/02/$ – see front matter
PII: S0040-6031(01)00834-6

ammonium oxalate ($(NH_4)_2C_2O_4$), ammonium hydroxide (NH_4OH) and glacial acetic acid were used for the preparation of oxalate.

2.2. Preparation of oxalate

Oxalates of La(III) from LaAc was prepared by dropwise addition of a hot 4% ammonium oxalate solution to a stirred hot solution of acetates after their dissolution in glacial acetic acid then neutralized to pH = 7 with (1:1) NH_4OH. The precipitates formed were left to stand at room temperature for 1 h, filtered off, washed with a diluted ammonium oxalate solution and finally dried at 80 °C to a constant weight.

The calcination products were obtained by heating at various temperatures 200–800 °C, in a static atmosphere of air for 1 h. The calcination temperatures were chosen on basis of the thermal analysis results. The calcination products indicate throughout the text by the oxalate designation and the temperature applied, thus LaOx-800 indicates the calcination product at 800 °C. The abbreviation WL stands for weight loss.

2.3. Thermal analysis

TG and DTA of lanthanum oxalate were carried out on heating at various rates (θ = 5, 10, 20, 30 °C/min) up to 900 °C in a dynamic atmosphere of air (20 ml/min), using a 7-series thermal analysis model Perkin-Elmer Analyzer. Ten to fifteen milligrams portions of the test sample were used for the TG measurements, and highly sintered α-Al_2O_3 was the thermally inert reference for the DTA. Shifts experienced by the DTA peak temperature (T_{max}) as a function of the heating rate (θ) were implemented to calculate the activation energy, ΔE (kJ/mol) corresponding to each of the thermal events monitored, according to the following equation [9]:

$$\Delta E = -\frac{R}{bd \log \theta d}\left(\frac{1}{T_{max}}\right)$$

where R is the gas constant (=8.314 kJ/mol) and b is a unitless constant (=0.457).

2.4. Infrared spectroscopy

IR-spectra were obtained at a resolution of 4 cm^{-1}, over the range 4000–400 cm^{-1}, using a model FT-IR-410 JASCO (Japan). IR-spectra of LaOx and its solid calcination products were obtained from thin (>20 mg/m^2), lightly loaded (<1%) KBr-supported discs.

2.5. X-ray diffraction

X-ray diffraction (XRD) powder patterns were obtained with JSX-60P JEOL diffractometer (Japan). The X-ray generator is equipped with Ni-filter and generates a beam of Cu Kα radiation (λ = 1.5418 Å). The operational settings for all the XRD scans are voltage: 40 kV, current: 30 mA, range: 4–60° (2θ), scanning speed: 8°/min, slit width: 0.02°. For identification purpose, the relative intensities (I/I^0) and the d-spacing (Å) are compared to standard diffraction patterns in the ASTM powder diffraction file [10].

2.6. N_2-adsorption measurements

N_2 sorption isotherms were determined volumetrically at −195 °C using a micro apparatus based on the design, which was described by Lippens et al. [11]. Test samples were outgassed at 220 °C for 6 h while evacuation at 10^{-5} Torr was performed. The reproducibility of the isotherm measurements was better than 97%.

3. Results and discussion

3.1. Characterization of the decomposition course

TG and DTA curves (Fig. 1) monitor 12 WL events (designated I–XIII) in the decomposition course of $LaOx{\cdot}10H_2O$, only three of these events are exothermic (event IX, X and XI), whereas the others are endothermic. The WL effected via the first eight events (I–VIII) accounts for a stepwise dehydration of $LaOx.10H_2O$, in which event I and II (WL = 2.7%, T_{max} = 86 °C) and (WL = 5.2%, T_{max} = 110 °C), respectively, each involves the elimination of 1 mol of water, and thermal event III (WL = 9.9%, T_{max} = 130 °C) leads to the removal of another 2 mol of H_2O. Events (IV–VII) (WL = 12.5, 15, 17.5, 20%) and (T_{max} = 155, 174, 195, 225 °C), respectively leads to the removal of another 4 mol of water. The corresponding activation energy values

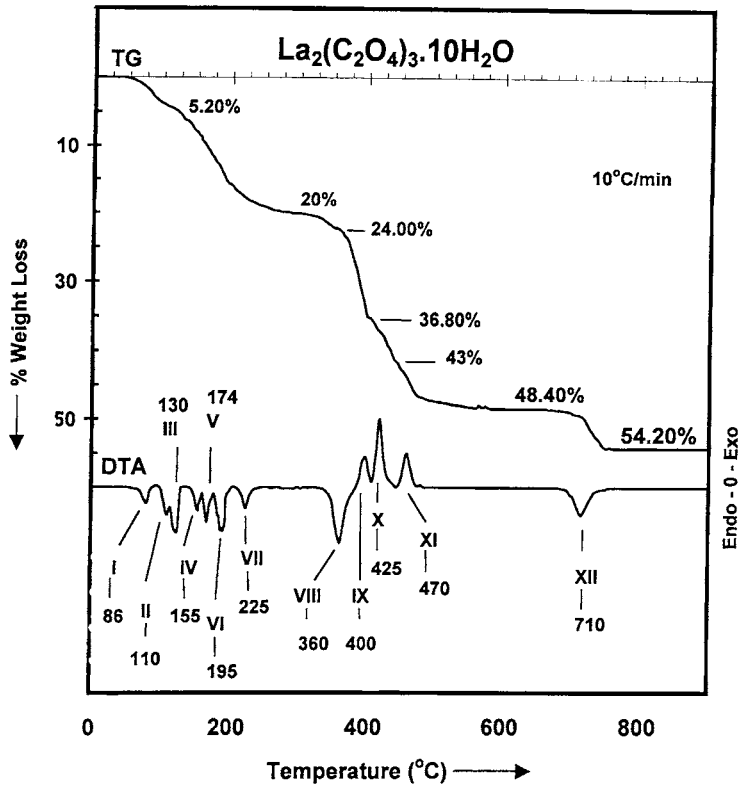

Fig. 1. TG and DTA curves recorded for LaOx at the heating rates indicated, in a dynamic (20 ml/min) atmosphere of air.

(Table 1) are well within the range (<60 kJ/mol) encountered for removal of weakly bound water of crystallization from analogous compounds [12]. The dihydrate thus formed, $LaOx{\cdot}2H_2O$, persists upon further heating to 300 °C at which event VIII ($T_{max} = 360$ °C) commences to operate. The total WL effected at 380 °C, (ca. 24%) accounts for the elimination of the remaining $2H_2O$ and, consequently, for the formation of the unhydrous lanthanum oxalate. The IR-spectrum of the solid phase LaOx-200 (Fig. 2) bears a great deal of similarity to that of unheated $La_2(C_2O_4)_3{\cdot}10H_2O$ because both show absorption bands arising from oxalate anions (at 1750–640 cm^{-1}) and water of hydration (at 3440 and 1640 cm^{-1}) [12,13]. However, the corresponding XRD pattern (Fig. 3) indicates that the products are amorphous and so water of hydration is very important for the coherency of LaOx crystal [14].

Table 1
Thermal processes; temperature (°C), composition and activation energy (ΔE, kJ/mol) proposed in each process for $LaOx{\cdot}10H_2O$

Process	Temperature (°C)	Composition	ΔE (kJ/mol)
I	86	$La_2(C_2O_4)_3{\cdot}9H_2O$	41
II	110	$La_2(C_2O_4)_3{\cdot}8H_2O$	43
III	130	$La_2(C_2O_4)_3.7H_2O$	94
IV	155	$La_2(C_2O_4)_3.6H_2O$	43
V	174	$La_2(C_2O_4)_3{\cdot}5H_2O$	51
VI	195	$La_2(C_2O_4)_3{\cdot}4H_2O$	54
VII	225	$La_2(C_2O_4)_3{\cdot}2H_2O$	60
VIII	360	$La_2(C_2O_4)_3$	108
IX	400	$La_2(CO_3)_3$	127
X	425	$La_2O(CO_3)_2$	123
XI	470	$La_2O_2CO_3$	145
XII	710	La_2O_3	254

The LaOx-300 solid phase IR-spectrum (Fig. 2) shows that the $C_2O_4^{2-}$ species are weakened and different band structure including absorptions at 2350 cm^{-1} and between 1800 and 400 cm^{-1} which is similar in shape and position to characteristic absorptions CO_3^{2-} [12].

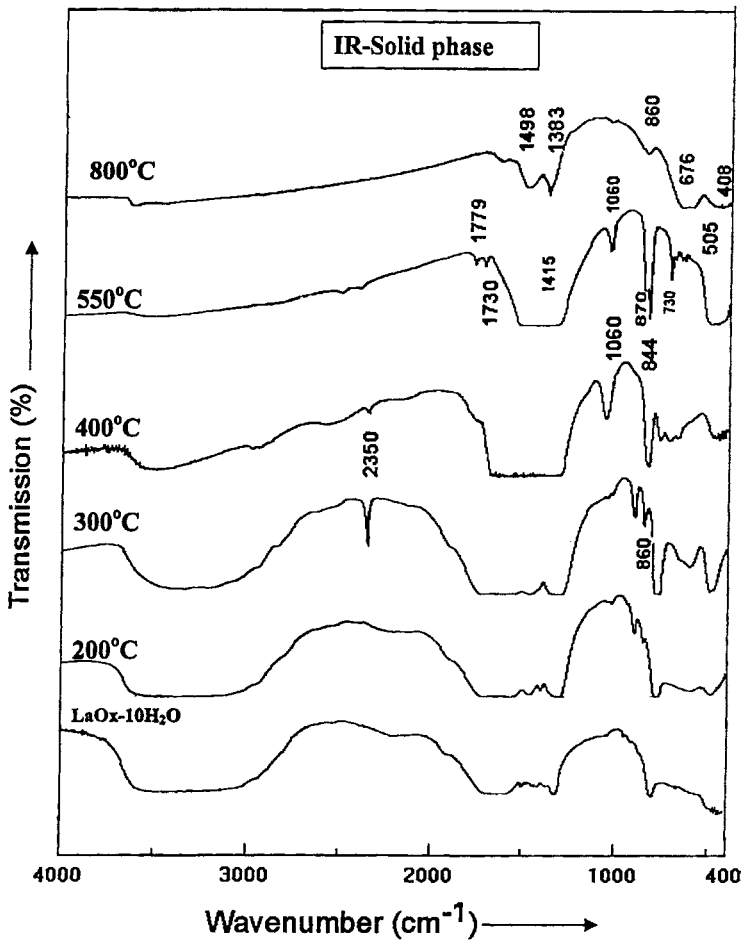

Fig. 2. IR-solid phase spectra for LaOx and its 1 h calcination products at the temperatures indicated.

Upon further heating event VIII is overlapped by two rapid exothermic WL processes (event IX, T_{max} = 400 °C and event X, T_{max} = 425 °C). The WL for IX is 36.9% which is close to that theoretically calculated (36.6%) for the formation of $La_2(CO_3)_2$, as follows:

$$La_2(C_2O_4)_3 \rightarrow La_2(CO_3)_3 \quad (1)$$

The IR-spectrum of LaOx-400 shows relived of the δHOH absorption of hydration of water [13], which is strong, broad absorption observed in the spectrum of both the parent, LaOx-200 and LaOx-300 between 1600 and 1750 cm^{-1}. The fundamental modes of vibration of the CO_3^{2-} species between 1800 and 400 cm^{-1} are weakened and different band structure begin to appear between 1600 and 1300 cm^{-1} which is similar in shape and position to characteristic absorptions of oxycarbonates [13]. XRD pattern for LaOx-400 (Fig. 3), reveals that the $La_2(CO_3)_3$ product inferred from the TG and IR-data is amorphous.

The WL for event X is 42.5% (expected WL is 42.7%) accounts for the conversion of $La_2(CO_3)_3$ to $La_2O(CO_3)_2$ which converts immediately to $La_2O_2CO_3$ (thermal event XI, WL = 48.4%, T_{max} = 470 °C) (Fig. 1), as follows:

$$La_2(CO_3)_3 \rightarrow La_2O(CO_3)_2 \rightarrow La_2O_2CO_3 \quad (2)$$

Events IX, X and XI must have overlapped between 420 and 550 °C. The similarity of the activation energy values (Table 1) for process IX, X and XI justifies their overlapping.

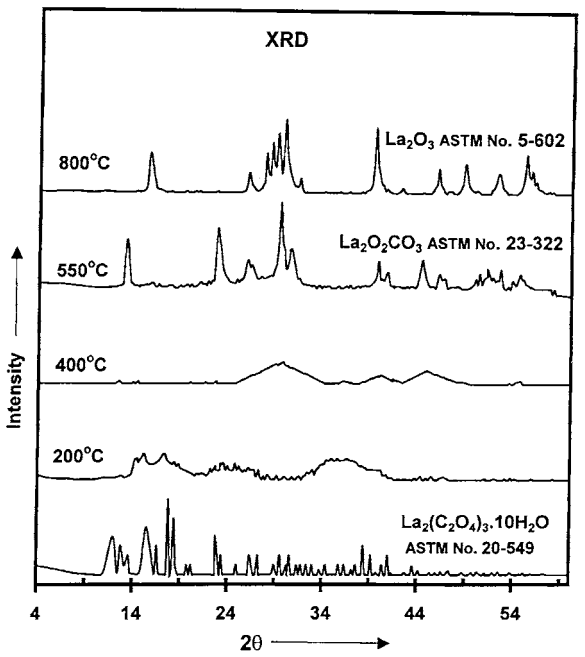

Fig. 3. X-ray powder diffractograms for LaOx and its 1 h calcination products at the temperatures indicated.

The IR-spectrum (Fig. 2) and XRD patterns (Fig. 3) support reaction (2). The IR-spectrum LaOx-550 displays strong absorptions between 1600 and 1300 cm^{-1} and also at 1060 and 870 cm^{-1} assignable to oxycarbonate species [13]. The absorption appearing at 730–500 cm^{-1} are related to La–O vibrational lattice mode [15].

The corresponding XRD pattern for LaOx-550 shows the pattern for crystalline $La_2O_2CO_3$ (ASTM no. 23-320).

At <600 °C, process XI slows down ending up with a weight invariant behavior at 670 °C. Process XII takes place endothermally at $T_{max} = 710$ °C. The maximum WL determined (54.2%) agrees well with that expected (54.8%) to accompany the overall conversion of $LaOx{\cdot}10H_2O$ to La_2O_3, i.e. process XII include the following pathway:

$$La_2O_2CO_3 \rightarrow La_2O_3 \quad (3)$$

Table 1 indicates that event XII has the highest activation energy ($\Delta E = 254$ kJ/mol) in the overall decomposition course of $LaOx{\cdot}10H_2O$, a fact that justifies its lowest kinetics.

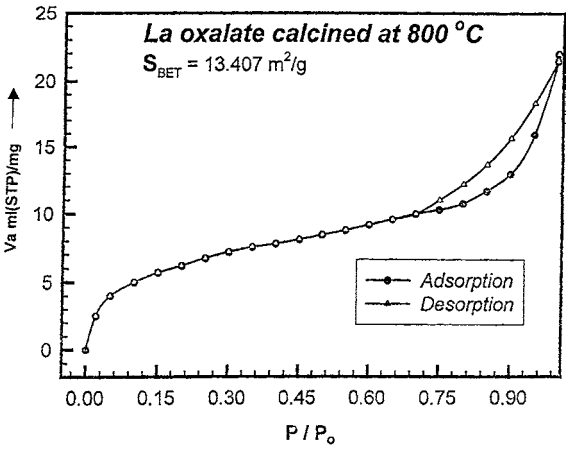

Fig. 4. N_2-adsorption isotherm obtained at −195 °C (using BET Method) for LaOx-800.

The IR-spectrum of LaOx-800 (Fig. 2), shows no detectable absorptions due to oxycarbonate species. The absorptions below 700 cm^{-1} are related to lattice vibration modes of La_2O_3 [15]. The weak bands around 1600, 1500 and 1380 cm^{-1} are most probably due to surface contamination by carbonate and moisture since it is known that La_2O_3 is a basic oxide [16].

In support, the XRD pattern of LaOx-800 detect a crystalline phase of La_2O_3 (ASTM no. 5-602).

3.2. Nitrogen sorption and surface area measurement of La_2O_3

The N_2-adsorption isotherm of LaOx-800 is shown in Fig. 4. The isotherm generally belongs to type IV of BET classification [17]. The desorption isotherm closed at $P/P^0 > 0.4$, which give indication the hysteresis loop is nearly of type H3 [17]. The loop suggested that the surface pores are of slit-shaped or interplating [18]. The S_{BET} value determined was 13.4 m^2/g.

4. Conclusion

The results of the present studies allow the following conclusions to be drawn:

1. The thermal decomposition course of hydrated lanthanum oxalate may include the following path

ways:

$$La_2(C_2O_4)_3 \cdot 10H_2O \xrightarrow{I} La_2(C_2O_4)_3 \cdot 9H_2O$$
$$\xrightarrow{II} La_2(C_2O_4)_3 \cdot 8H_2O \xrightarrow{III} La_2(C_2O_4)_3 \cdot 6H_2O$$
$$\xrightarrow{IV} La_2(C_2O_4)_3 \cdot 5H_2O \xrightarrow{V} La_2(C_2O_4)_3 \cdot 4H_2O$$
$$\xrightarrow{VI} La_2(C_2O_4)_3 \cdot 3H_2O \xrightarrow{VII} La_2(C_2O_4)_3 \cdot 2H_2O$$
$$\xrightarrow{VIII} La_2(C_2O_4)_3 \xrightarrow{IX} La_2(CO_3)_3 \xrightarrow{X} La_2O(CO_3)_2$$
$$\xrightarrow{XI} La_2O_2CO_3 \xrightarrow{XII} La_2O_3.$$

2. The lower hydrate oxalate (dihydrate) is thermally stable but the unhydrous oxalate is unstable and the water of hydration is responsible of the crystal coherency of LaOx.
3. Lanthanum carbonates $La_2(CO_3)_3$ (amorphous), $La_2O(CO_3)_2$ (amorphous), $La_2O_2CO_3$ (crystalline), were formed as intermediates during the decomposition of lanthanum oxalate hydrate but with no region of stability.
4. A crystalline phase of La_2O_3 were detectable as the final decomposition product of $La_2(C_2O_4)_3$.
5. La_2O_3 obtained at 800 °C has a surface area of 13.4 m^2/g.

References

[1] P. Kofstad, Nonstoichiometry, Diffusion and Electrical Conductivity in Binary Metal Oxide, Wiley, New York, 1972, p. 289
[2] M. Hideaki, S. Hirofami, S. Hideo, F. Yoshiyasu, Ind. Eng. Chem. Proc. Res. Dev. 25 (2) (1988) 202.
[3] D. Andriamasinoro, R. Kieffer, A. Kiennemann, P. Poix, Appl. Catal. 106 (1993) 201.
[4] M.P. Rosynek, D.T. Magnison, J. Catal. 46 (1977) 402.
[5] K. Okabe, K. Sayama, H. Kusama, H. Arakawa, Bull. Chem. Soc. Jpn. 67 (1994) 2894.
[6] K. Otsuka, K. Jinno, A. Morikawa, J. Catal. 100 (1986) 353.
[7] H. Arakawa, Bull. Chem. Soc. Jpn. 21 (11) (1994) 31.
[8] N.I. Sax and R.J. Lewis (Eds.), Hawley's Condensed Chemical Dictionary, 11th Edition, Reinhold, New York, 1987, p. 683.
[9] J.H. Flynn, J. Thermal. Anal. 27 (1983) 45.
[10] J.V. Smith (Ed.), X-ray Powder Data File, American Society for Testing and Materials, PA, USA, 1960.
[11] B.C. Lippens, B.G. Linsen, J.H. De Boer, J. Catal. 3 (1964) 32.
[12] M.E. Brown, D. Dollimore, A.K. Galwey, in: C.H. Bamford, C.F.H. Tipper (Eds.), Chemical Kinetics, Reaction in the Solid State, Elsevier, Amsterdam, 1980.
[13] K. Nakamoto, Infrared Spectra of Inorganic and Coordination Compounds, Wiley, New York, 1970, p. 253.
[14] G.A. Gadsden, Infrared Spectra of Minerals and Related Inorganic Compounds, Butterworths, London, 1975, p. 65.
[15] J.A. Goldsmith, S.D. Ross, Spectrochem. Acta Part A 23 (1967) 1909.
[16] K. Tanabe, K. Misono, Y. Ono, H. Hatori, New Solid Acids and Bases, Kodansha, Tokyo; Elseveir, Amsterdam, 1989, pp. 41–47.
[17] S.J. Gregg, K.S.W. Sing, Adsorption Surface Area and Porosity, 2nd Edition, Academic Press, London, 1982.
[18] K.S.W. Sing, Pure Appl. Chem. 54 (1982) 2201.